Symmetry-adapted configurational modelling of fractional site occupancy in solids

2007 J. Phys.: Condens. Matter 19 256201

(http://iopscience.iop.org/0953-8984/19/25/256201)

IOP PUBLISHING JOURNAL OF PHYSICS: CONDENSED MATTER

J. Phys.: Condens. Matter **19** (2007) 256201 (16pp) doi:10.1088/0953-8984/19/25/256201

Symmetry-adapted configurational modelling of fractional site occupancy in solids

R Grau-Crespo[1], S Hamad[1,2], C R A Catlow[1,2] and N H de Leeuw[1]

[1] Department of Chemistry, University College London, 20 Gordon Street, London WC1H 0AJ, UK
[2] Davy–Faraday Research Laboratory, The Royal Institution of Great Britain, 21 Albemarle Street, London W1S 4BS, UK

E-mail: r.grau-crespo@ucl.ac.uk

Received 24 January 2007, in final form 25 January 2007
Published 31 May 2007
Online at stacks.iop.org/JPhysCM/19/256201

Abstract

A methodology is presented, which reduces the number of site-occupancy configurations to be calculated when modelling site disorder in solids, by taking advantage of the crystal symmetry of the lattice. Within this approach, two configurations are considered equivalent when they are related by an isometric operation; a trial list of possible isometric transformations is provided by the group of symmetry operators in the parent structure, which is used to generate all configurations via atomic substitutions. We have adapted the equations for configurational statistics to operate in the reduced configurational space of the independent configurations. Each configuration in this space is characterized by its *reduced energy*, which includes not only its energy but also a contribution from its degeneracy in the complete configurational space, via an entropic term. The new computer program SOD (site-occupancy disorder) is presented, which performs this analysis in systems with arbitrary symmetry and any size of supercell. As a case study we use the distribution of cations in iron antimony oxide $FeSbO_4$, where we also introduce some general considerations for the modelling of site-occupancy disorder in paramagnetic systems.

1. Introduction

Site-occupancy disorder, defined as the non-periodic occupation of lattice sites in a crystal structure, is a ubiquitous phenomenon in solid-state chemistry. Relevant examples are metallic alloys, mineral solid solutions, and synthetic non-stoichiometric compounds. The experimental investigation of these materials using diffraction techniques or other methods developed for the study of periodic crystals only provides averaged information of their properties, thus mapping

the complexity of long-range patterns of site-occupancy configurations into a small crystal unit cell with ill-defined (fractional) site occupancies.

Computer-modelling techniques are well suited to make valuable contributions to the investigation of site-occupancy disorder in solids, by evaluating the relative stabilities of configurations using simple energetic criteria (e.g. [1–10]). Several computational strategies have been employed to this end, which usually involve the evaluation of the energies of different site-occupancy configurations in a supercell of the structure. One important limitation of the supercell approach is the computational cost. This problem is two-fold: first, the evaluation and minimization of the energy of a large supercell can be very expensive, even if interatomic potential methods rather than quantum-mechanical techniques are employed; and second, the number of possible configurations increases dramatically with the supercell size, quickly reaching very high values. The combination of these two limitations makes it very difficult to perform a direct study of the complete configurational ensemble for any supercell other than a very small, usually insufficient, simulation cell.

In order to deal with the first of the above-mentioned problems, one common strategy is to use simple parametric interaction models containing energy contributions for each pair of atom types in nearest-neighbour (NN) or next-nearest-neighbour (NNN) sites. The parameters of these interaction models are fitted to reproduce the energies obtained using quantum-mechanical or interatomic potential methods in small supercells. These simple interaction models perform remarkably well in some systems like metallic alloys, where the relevant interactions for site occupation are essentially short-range. They can also be applied successfully to the study of covalent solid solutions and of same-charge cation or anion distributions in ionic systems. However, when the site-occupation configurations differ in their charge distributions, as is the case in many ionic solid solutions, the effect of the long-range electrostatic interactions cannot simply be incorporated into NN and NNN potentials, and should be evaluated explicitly.

The second problem, relating to the number of configurations, is even more difficult to solve. One approach used by various authors (e.g. [8–10]), has been to sample the configurational space using the Monte Carlo method, where configurations are randomly generated, before being accepted or rejected in the ensemble according to the Metropolis algorithm [11]. In this way, it is possible to obtain a representative set of configurations, which can be considerably smaller than the complete configurational space.

An alternative approach to reduce the number of configurations is to take advantage of the system symmetry. Many configurations are symmetry related and therefore identical, so it is possible to limit the configurational space to the symmetrically inequivalent configurations only. This is the approach that we have used in recent studies [12, 13], and the methodology to implement this idea is fully described in the present paper. Todorov *et al* [10] have discussed an alternative methodology, which is based on the determination and comparison of the space group of the different structures. However, as the authors note, the fact that two configurations have the same space group does not imply that they will have the same energy. Having the same space group is a necessary but not a sufficient condition for two configurations to be symmetrically equivalent.

In this paper we present the conditions that are both necessary and sufficient to obtain the symmetry equivalence of two configurations, and its implementation in a computer program that identifies the different site-occupancy configurations for any structure with arbitrary supercell size, space group or composition. We also demonstrate the calculation of the thermodynamic properties of independent configurations in the reduced space. To illustrate our approach, we consider the case of the distribution of cations in iron antimony oxide $FeSbO_4$, where we discuss some aspects of the modelling of site-occupancy disorder in paramagnetic systems.

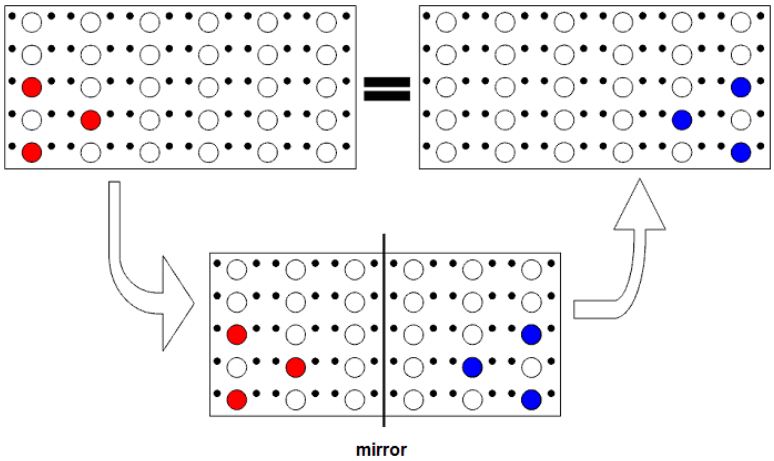

Figure 1. Illustration of identical configurations related by an isometric transformation. (This figure is in colour only in the electronic version)

2. Theoretical background and implementation

2.1. Equivalence between configurations

The criterion of equivalence between two configurations is based on the concept of isometric transformations [14], which are geometric operations (e.g. translations, rotations, reflections) that keep constant all the distances and angles within the transformed object. Thus, two configurations are considered equivalent if there is one isometric transformation that converts one into the other (figure 1).

In order to find the isometric transformation linking two equivalent configurations, it is possible to make use of the symmetry of the crystal. Symmetry operations in a crystal are defined as those isometric transformations which convert the structure into itself [14]. Although the isometric transformation that converts one configuration into the other is not a symmetry operator of any of the two equivalent structures, it has to be a symmetry operator of the *parent structure*, that is, the structure from which all configurations can be derived by effecting certain site substitutions. Therefore, in order to find out whether two given configurations are equivalent, it is sufficient to check if any of the symmetry operators of the parent structure converts one of the configurations into the other.

The implicit assumption here is that after relaxation each configuration will keep the same symmetry operators of the parent structure, except for the symmetry breaking caused by the substitution itself. In the case of dilute defects, the parent structure will clearly be the non-defective structure, but in general it is not possible to define the parent structure in terms of homogeneous occupation of the substitution sites in one of the end-member structures, which may exist only with a different crystal structure. The best definition of the parent structure is in terms of the experimental averaged crystal lattice, provided that this is known beforehand. For example, when studying the cation distribution in $FeSbO_4$ (see section 3 and [12, 13]), we cannot take the pure oxides as reference structures, as they crystallize in completely different lattice types. In this case we must use the experimental crystal structure, which for $FeSbO_4$ is a rutile-like structure [15].

We note that in the present methodology, we focus on the symmetry of the parent structure rather than the approach followed by Todorov *et al* [10], which considers the symmetry group of each particular configuration. The equivalence criterion presented here is more restrictive: if two configurations are related by an isometric transformation, then they have the same symmetry group, but the opposite is not necessarily true.

2.2. Symmetry operators in an arbitrary supercell

We now consider the general problem of identifying all the symmetry operators in an arbitrary supercell, which form the pool of isometric transformations that will be explored to check equivalencies between configurations. Although the symmetry of any crystal structure can be described by one of the 230 crystallographic space groups, all the symmetry information of the supercell is not contained in the space group description, as translations are not included once a supercell is created. However, if we know the symmetry operators in the space group of the unit cell, and the number of repetitions (N_1, N_2, N_3) of the unit cell in each direction which define the supercell $N_1 \times N_2 \times N_3$, it is possible to find the set of all the symmetry operators of the supercell.

We will use here the matrix–vector representation of the operators: for each operator $\widehat{O}$ of the space group there is a matrix $\overline{\overline{O}}$ and a vector $\overline{o}$ such that the action of the operator on the fractional coordinates of an arbitrary point is

$$\widehat{O}\bar{x} = \overline{\overline{O}} \cdot \bar{x} + \bar{o} = \begin{pmatrix} O_{11} & O_{12} & O_{13} \\ O_{21} & O_{22} & O_{23} \\ O_{31} & O_{32} & O_{33} \end{pmatrix} \begin{pmatrix} x_1 \\ x_2 \\ x_3 \end{pmatrix} + \begin{pmatrix} o_1 \\ o_2 \\ o_3 \end{pmatrix}. \tag{1}$$

If the supercell shape is consistent with the space group of the structure ($N_1 = N_2 = N_3$ for cubic space groups, $N_1 = N_2$ for tetragonal space groups, etc), then the supercell will have the same symmetry elements as the unit cell. In the matrix–vector representation, the components of the matrix will remain the same, but the components of the vector must be rescaled to reflect the change in the length of the cell vectors:

$$o_i' = \frac{o_i}{N_i}, \qquad i = 1, 2, 3. \tag{2}$$

On the other hand, if the supercell shape is not consistent with the space group, some operators of the original group should be excluded from the supercell group. The rule is that if $N_i \neq N_j$, all operators containing matrix elements $O_{ij} \neq 0$ must be excluded, as these operators 'mix' the two directions that are no longer equivalent because of the supercell shape.

Not only the space-group symmetry elements, but also the internal translational symmetry, contribute to the symmetry of the supercell. For the internal translations $\widehat{T}$ the operator matrix is simply a unity matrix:

$$\overline{\overline{T}} = \overline{\overline{I}} = \begin{pmatrix} 1 & 0 & 0 \\ 0 & 1 & 0 \\ 0 & 0 & 1 \end{pmatrix} \tag{3}$$

and the operator vectors are

$$\bar{t} = \begin{pmatrix} n_1/N_1 \\ n_2/N_2 \\ n_3/N_3 \end{pmatrix} \tag{4}$$

where $n_i = 0, \ldots, N_i - 1$ (there are $N_1 \times N_2 \times N_3$ translational operators). We also have to include all the combinations between the symmetry elements of the unit cell space group and these internal translation operations. Therefore, if the supercell shape is consistent with

the symmetry of the unit cell, the number of symmetry operators in the supercell (N_O) is $N_1 \times N_2 \times N_3 \times N_{SG}$, where N_{SG} is the number of operators in the unit cell space group. If the supercell is not consistent with the unit cell symmetry, the number of operators in the supercell will be smaller than that.

Having obtained the group of symmetry operators of the supercell, we can find all the equivalent configurations within the complete space of N configurations, thus identifying M independent configurations, where in general $M \ll N$. As a result we can then restrict our classical or quantum-mechanical calculations to this set of M independent configurations, which from now on we will call *reduced configurational space*. In general, the larger the number of symmetry operators N_O, the smaller the proportion of independent configurations, although the number of configurations is not necessarily reduced by a factor N_O as in many cases an operator converts a configuration into itself (for example, a configuration that is symmetrically arranged at both sides of a plane does not change under the action of a reflection by that plane). Therefore, the *degeneracy* Ω_m of each independent configuration m ($m = 1, M$), which is the number of configurations in the complete space that are equivalent to the independent configuration m, depends on the symmetry of the configuration.

2.3. Implementation in the SOD program

We have implemented the above ideas in a computer program, SOD (Site-Occupancy Disorder), which was written in the Fortran90 language. The algorithm used in the program to obtain the list of independent configurations, I, from the list of all the configurations, A, is represented in the flow charts of figure 2. A loop is performed through all the configurations in the list A (see figure 2(a)). The list I, which initially contains just the first configuration, is populated at each step with a particular configuration from A if the configuration is found to be independent of those already included in I. In order to check this independence, we use an auxiliary list E, which at each step contains the independent configurations already found, plus all their equivalent configurations. Finally, the list E will contain the complete set of configurations. The calculation of all the configurations that are equivalent to a particular independent configuration is performed by a secondary loop, which is explained in figure 2(b).

The program can therefore determine whether a particular configuration in A is a new independent one, just by checking whether the configuration is included in E. If this is not the case, the configuration is added to I, and together with all its equivalent configurations, also to E. Then the number of equivalent configurations is counted, which is the degeneracy of the independent configuration. The same procedure is repeated for the next configuration, until E contains all the configurations ($E = A$). At the end of the process, the list I will contain only the non-equivalent configurations.

2.4. Configurational statistics

We now show how to obtain the thermodynamic properties associated with configurational disorder from the results of the calculations in the reduced configurational space. We first summarize the equations for configurational statistics in the complete space of all configurations. If all site-occupancy configurations are in thermodynamic equilibrium at temperature T, each configuration n in the complete space ($n = 1, \ldots, N$) can be assigned an occurrence probability:

$$P_n = \frac{1}{Z} \exp(-E_n / k_B T), \tag{5}$$

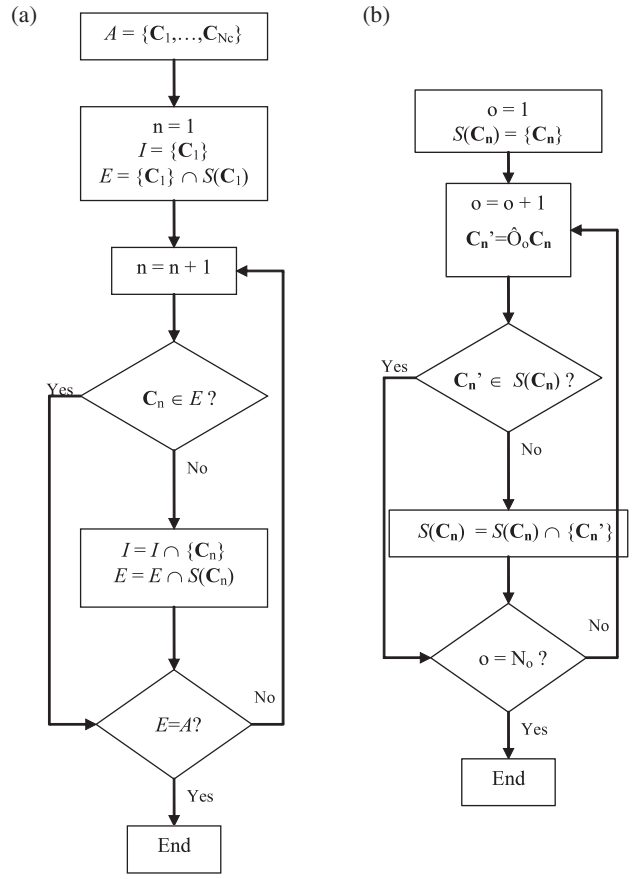

Figure 2. Flow charts explaining the operation of the SOD program. (a) Main part of the code, which identifies the list of independent configurations. Cursive capital letters represent groups of configurations. A is the group of all configurations, I the group of independent configurations and E the group of equivalent configurations, which initially is formed by the first configuration in A, $\{C_1\}$, plus the group of all its equivalent configurations, $S(C_1)$, which are all the configurations obtained by applying each of the symmetry operations to that configuration. n and o are integer indices, n running from 1 to N_c, the total number of configurations, while o runs from 1 to N_o, the total number of symmetry operations. (b) Secondary part of the code, which is where the list of configurations equivalent to C_n, $S(C_n)$, is calculated, by multiplying the vector associated with C_n by $\hat{O}o$, the symmetry operator matrix. If C_n' is not included in the group of equivalent configurations, $S(C_n)$, it is then added, so that when the last symmetry operator, $\hat{O}$ N_o, is applied, $S(C_n)$ includes all the equivalent configurations, without repetitions.

where $k_B = 8.6173 \times 10^{-5}$ eV K^{-1} is Boltzmann's constant, E_n is the energy of that configuration and

$$Z = \sum_{n=1}^{N} \exp(-E_n/k_B T) \tag{6}$$

is the partition function. Now, we can calculate the energy of the system in configurational equilibrium as the average:

$$E = \sum_{n=1}^{N} P_n E_n, \tag{7}$$

while the configurational free energy can be obtained from the partition function as

$$F = -k_B T \ln Z \tag{8}$$

and therefore the configurational entropy is simply

$$S = \frac{E - F}{T}. \tag{9}$$

In the case of a perfectly ordered system, in which one non-degenerate configuration has a much lower energy than the rest, both the energy and the free energy of the system are identical to the energy of that configuration, and the configurational entropy is zero. Alternatively, for a totally disordered system of N configurations, all with identical energies, the configurational entropy reaches a maximum value:

$$S_{\max} = k_{\mathrm{B}} \ln N. \tag{10}$$

Generally, however, the configurational entropy calculated by equation (9) can take any value between zero and $S_{\max}$, depending on the temperature and on the energy distribution of the configurations.

It should be noted that in the above equations all temperature effects have been excluded in the calculation of the energies and partition function; in particular the vibrational contribution to the stability of the configurations has been ignored. It is possible to calculate this vibrational entropy term, S_{vib}, by standard lattice dynamical procedures [16], and thus to replace the energy, E_n, of each configuration by its corresponding Helmholtz free energy term: $F_n^{\mathrm{vib}} = E_n - T S_{\mathrm{vib}}$. In this case, the entropy calculated with equation (9) will contain both configurational and vibrational contributions. Analogously, we can consider the effect of finite pressures and volume differences between configurations, by adding the term pV_n to the energy of each configuration, that is, by using the Gibbs free energy instead of the Helmholtz free energy (and average enthalpies instead of average energies). This complete formulation has been used and explained in detail by Allan *et al* in their studies of MgO/MnO [10] solid solutions.

Now we can translate the above equations to the reduced configurational space. The probability $\tilde{P}_m$ of an independent configuration m ($m = 1, \ldots, M$) with degeneracy Ω_m occurring is

$$\tilde{P}_m = \frac{1}{Z}\Omega_m \exp(-E_m/k_B T) = \frac{1}{Z}\exp(-\tilde{E}_m/k_B T) \tag{11}$$

where we have introduced the *reduced energy*:

$$\tilde{E}_m = E_m - T S_m \tag{12}$$

which can be seen as a temperature-dependent free energy associated with the *degeneracy entropy*:[3]

$$S_m = k_B T \ln \Omega_m. \tag{13}$$

The introduction of this degeneracy entropy allows us to take into account the effect of the configuration degeneracy and to make direct comparisons of independent configurations via the reduced energies, which comprise both the energetic and the degeneracy information. In particular, from the previous equations it is clear that, if two independent configurations have the same energy, the one with higher degeneracy will have higher degeneracy entropy, which

[3] In [12, 13] the term configurational entropy was used to denote what we call here degeneracy entropy, which is a property defined for each individual configuration. This was misleading, as the term configurational entropy has been used traditionally to denote the entropic contribution from disorder to the stability of a system, and refers to the whole system in configurational equilibrium, rather than to one particular configuration. In this paper we employ the traditional terminology.

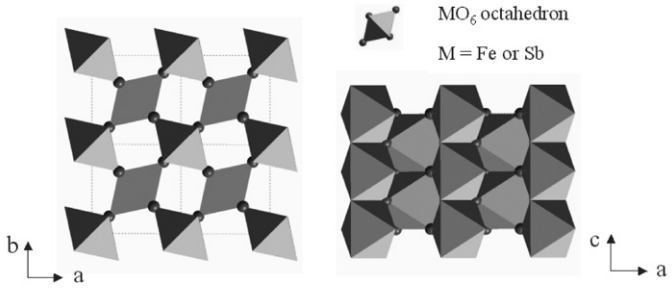

Figure 3. The crystal structure of $FeSbO_4$, showing the octahedral coordination of the cations.

in turn lowers its reduced energy $\tilde{E}_m$, resulting in a higher probability of appearance for that configuration.

The energy and the partition function can therefore be calculated in the reduced space as

$$E = \sum_{m=1}^{M} \tilde{P}_m E_m \tag{14}$$

and

$$Z = \sum_{m=1}^{M} \exp(-\tilde{E}_m / k_B T) \tag{15}$$

which allows the calculation of the configurational entropy via equation (9).

Finally, it is worth noting that, in the equations above, T is the temperature at which the configurations are in equilibrium. However, cation exchange is often inhibited by high activation barriers, and thermodynamical equilibrium, except at high temperatures, should not be expected. Farber *et al* [17], for example, have shown that, in the perovskite solid solution $Pb(Mg_{1/3}Nb_{2/3})O_3$–$Pb(Sc_{1/2}Nb_{1/2})O_3$, the distribution of cations is thermodynamically controlled only above ∼1330 K. This threshold temperature, whenever known, should be used to calculate the site-occupancy distributions for any temperature below that value.

3. A practical example: cation disorder in $FeSbO_4$

3.1. Structure description and calculation details

In this section we present the results of the application of the above methodology to the study of the cation distribution in the iron (III) antimony (V) oxide $FeSbO_4$. This structure is described in terms of a rutile-like framework with Fe and Sb cations distributed in the octahedral sites within the oxygen lattice (figure 3). Most experimental studies have concluded that the cation distribution is completely disordered (see [15] for a review), although some diffraction data have also been interpreted in terms of partial cationic ordering in a supercell with triple c parameter compared to common rutile [18, 19]. However, a recent computer-modelling study of the cation distribution found that Fe and Sb cations show a clear preference to alternate along the c-axis of the crystal, while these chains of alternating cations connect laterally with significant disorder in the a–b plane, which prevents three-dimensional long-range ordering [13]. We will report here the results of a more rigorous study of the cation distribution in this material, which will allow us to evaluate the validity of previous assumptions and

Table 1. Number of independent configurations for a series of supercells of $FeSbO_4$.

Supercell	Number of symmetry operations N_o	Total number of configurations N	Number of independent configurations M
$1 \times 1 \times 1$	16	2	1
$1 \times 1 \times 2$	32	6	2
$1 \times 1 \times 3$	48	20	3
$1 \times 1 \times 4$	64	70	8
$2 \times 2 \times 1$	64	70	7
$2 \times 2 \times 2$	128	12 870	180

approximations, and we will use this example to illustrate the calculation of the thermodynamic properties associated with configurational disorder according to the methodology introduced above.

We used the SOD program to obtain all the different substitutions of Fe and Sb in the cationic sites of different supercells of the rutile structure (table 1), before calculating the energies for the configurations in the reduced space and performing the statistical analysis for two supercells: $1 \times 1 \times 2$ and $2 \times 2 \times 2$.

All the energies were obtained using the density functional theory (DFT) as implemented in the Vienna *Ab Initio* simulation program (VASP) [20–23], with a generalized-gradient approximation (GGA) functional built from the Perdew and Zunger [24] local functional, with the spin interpolation formula of Vosko *et al* [25] and the gradient corrections by Perdew *et al* [26]. The interaction between the valence electrons and the core was described with the projected augmented wave (PAW) method [27] in the implementation of Kresse and Joubert [28]. The core levels, which were kept frozen during the calculations, consisted of orbitals up to, and including, the 3p levels for Fe, the 4d levels for Sb and the 1s level for oxygen.

It is well known that the GGA approximation fails in the description of the electronic properties of several transition metal compounds, as the electron self-interaction error becomes significant for electrons in the well-localized d levels of the transition metals. In this work we have therefore used the DFT + U methodology [29–32], which combines the DFT and a Hubbard Hamiltonian to account for the intra-atomic Coulomb repulsion, which is not well described in standard DFT. We use here the simple formulation by Liechtenstein *et al* [31] and Dudarev *et al* [32], where a single parameter, U_{eff}, determines an orbital-dependent correction to the DFT energy. U_{eff} is generally expressed as the difference between two parameters, the Hubbard U, which is the Coulomb-energetic cost to place two electrons at the same site, and an approximation of the Stoner exchange parameter I, which is almost constant at ∼1 eV [33]. The DFT + U correction alters the one-electron potential locally for the specified orbitals of the metal atoms (e.g. Fe d orbitals), reducing the hybridization with the ligands (e.g. O atoms). The $U_{\text{eff}} = 0$ case represents the DFT limit. Details of the implementation of the DFT + U method in the VASP code can be found in the work by Rohrbach *et al* on transition metal sulfides. In a previous paper [34] it was shown that the GGA + U methodology with $U_{\text{eff}} = 4$ eV provides an adequate description of the electronic structure and the magnetic interactions in $FeSbO_4$, in contrast with pure GGA, which predicts too high a magnetic coupling, too narrow a band gap and a pressure-induced Fe spin transition without experimental support. Previous studies have also shown that GGA + U provides an adequate description of the defect chemistry and surface properties of $FeSbO_4$ [35, 36]. In the present work we use the same value $U_{\text{eff}} = 4$ eV in all calculations.

We note that the calculation details here are different from those in our previous study [13] of the cation distribution in $FeSbO_4$, where ultrasoft pseudopotentials were employed and no

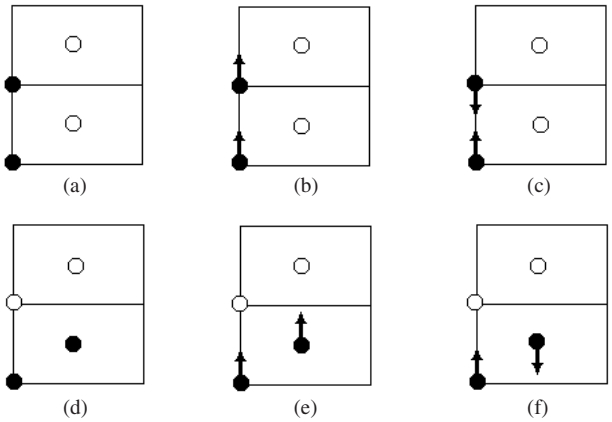

Figure 4. Scheme of the non-magnetic (a), (d), ferromagnetic (b), (e) and antiferromagnetic arrangements (c), (f) for configurations 1 (above) and 2 (below) for the $1 \times 1 \times 2$ supercell. Solid and open circles represent Fe and Sb cations respectively. Oxygen positions are omitted for clarity.

DFT + U correction was applied. More importantly, no spin polarization was included in this previous work, as it was argued there that, at the temperatures at which the cationic ordering occurs (a typical synthesis temperature is 1273 K), no magnetic order is present in the material, and therefore the introduction of spin polarization with arbitrary ordering of the magnetic moments would lead to artificial energy differences between configurations. Although it is true that magnetic ordering is only present at very low temperatures (Néel temperature is ∼1 K in $FeSbO_4$) and therefore does not contribute to the evolution of the cationic distribution at relevant temperatures, even so we will show here that non-spin polarized energies are not a good representation of the paramagnetic phase. We will present a different method, based on the use of a spin model Hamiltonian, to obtain the paramagnetic energies while retaining the spin-polarized character of the calculations.

3.2. The $1 \times 1 \times 2$ *supercell*

The $1 \times 1 \times 2$ is the simplest supercell that can provide useful information about the cation distribution. The extension along the c-axis is chosen, since $c < a$ and the interactions between cations of neighbouring cells are likely to be more important in that direction, especially as the octahedra in the c-direction are edge-sharing rather than corner-sharing. Only two different distributions of cations are possible in this supercell. The first configuration (figure 4(a)) corresponds simply to the repetition of the same ordered unit cell in the c-direction, whereas the second (figure 4(b)) has the two Fe cations in one cell (bottom) and the two Sb cations in the second cell (above).

Table 2 shows the results of the calculations of the $1 \times 1 \times 2$ supercell, where we have obtained spin-polarized solutions with the nearest-neighbour magnetic moments aligned both in parallel directions (ferromagnetic phase, FM) and in antiparallel directions (antiferromagnetic phase, AF). For both magnetic arrangements configuration 2 has a lower energy than configuration 1, in agreement with our previous results without spin polarization [12, 13], where it was concluded that the alternation of different cations along the c-axis is much more favourable than having vertical chains of identical cations. The higher relative stability of cation alternation is reinforced by the contribution from the degeneracy entropy, which is larger for configuration 2 than for configuration 1.

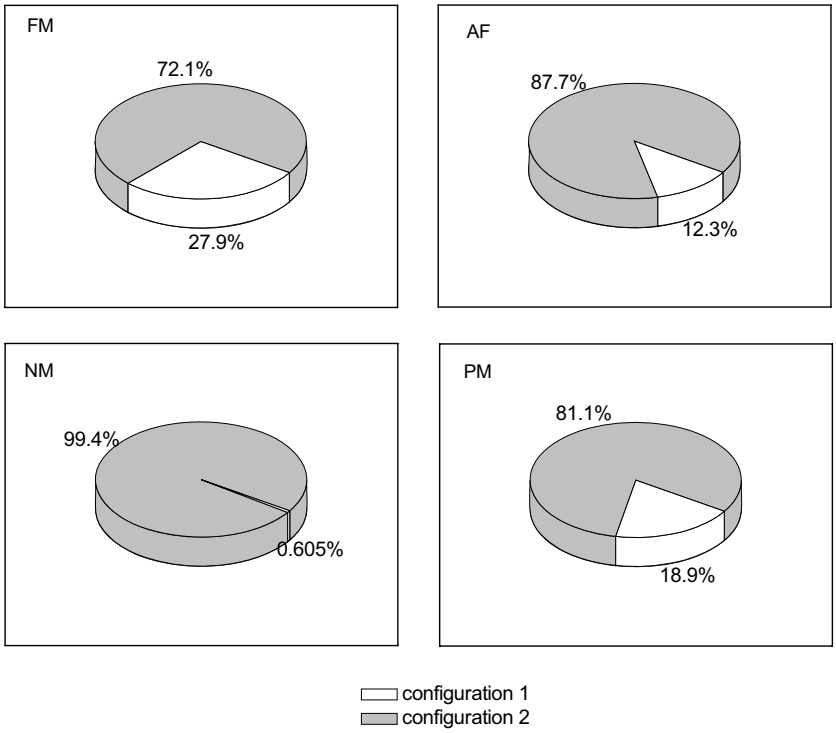

Figure 5. Probabilities of formation at $T = 1273$ K for configurations 1 and 2 in the $1 \times 1 \times 2$ supercell, obtained from ferromagnetic (FM), antiferromagnetic (AF), non-magnetic (NM) and paramagnetic (PM) energies.

Table 2. Summary of the calculations in the $1 \times 1 \times 2$ supercell. The probabilities P are calculated using the reduced paramagnetic energies ($E_{\mathrm{PM}} - TS_d$) at $T = 1273$ K.

	Conf. 1	Conf. 2
E_{FM} (eV)	−77.564	−77.592
E_{AF} (eV)	−77.642	−77.782
E_{PM} (eV)	−77.603	−77.687
Ω	2	4
TS_d (eV)	0.076	0.152
P	0.189	0.811

It is important to note that the differences in energy between the two configurations in the present spin-polarized calculations are smaller than in the calculations without spin polarization (which was ∼0.5 eV) [12, 13]. In order to evaluate the effect of spin polarization in the estimation of relative stabilities, we have calculated the Boltzmann probabilities of the two configurations using non-magnetic (NM) and magnetic (FM and AF) energy differences, as shown in figure 5. From a negligible 0.6% probability for configuration 1, when no magnetic effects were considered, the probability increases to 12.3% and 27.9% when the system is AF and FM respectively, which suggests that the effect of spin polarization can indeed be significant. However, as we mentioned above, magnetic ordering is present only at very low temperatures, and, therefore, no contributions from magnetic ordering should be included in the calculation of the probabilities of the configurations, which does not mean that the NM energies

are correct at high temperatures, when the system is paramagnetic, because in the paramagnetic phase the iron ions are still spin-polarized. In order to exclude the contribution of magnetic ordering to the energy, whilst keeping the spin-polarized nature of the solution representing the high-temperature (paramagnetic) phase, we suggest following a simple procedure that has already been used by other authors in different contexts. The calculation of FM and AF energies allows us to obtain the magnetic coupling constants J_d and J_v, for diagonal (as in configuration 1) and vertical (as in configuration 2) Fe–Fe pairs, respectively, by mapping the calculated results onto a Heisenberg spin model:

$$E = E^{\mathrm{PM}} - 2\sum_{\langle i,j\rangle} J_{ij} S_i S_j \tag{16}$$

where $S = \pm 5/2$ in the case of high-spin Fe^{3+} ions, and the J values are the magnetic coupling constants. The E^{PM} value for each cation configuration is independent of the magnetic ordering and can be regarded as the energy of that cation configuration in the paramagnetic (PM) phase, as the contribution $\sum_{\langle i,j\rangle} J_{ij} S_i S_j$ is zero for a system of completely disordered spins. Applying the above equation to the magnetic states of configuration 1, we obtain

$$J_v = [E_1^{\mathrm{AF}} - E_1^{\mathrm{FM}}]/8S^2 = -18.2\ \mathrm{K} \tag{17}$$

and

$$J_d = [E_2^{\mathrm{AF}} - E_2^{\mathrm{FM}}]/16S^2 = -22.1\ \mathrm{K} \tag{18}$$

where E_1^{FM} and E_1^{AF} are the FM and AF energies of configuration 1, and E_2^{FM} and E_2^{AF} are the FM and AF energies of configuration 2. The negative values indicate antiferromagnetic coupling, in agreement with experimental evidence. The paramagnetic energies can now be calculated as

$$E_1^{\mathrm{PM}} = \tfrac{1}{2}(E_1^{\mathrm{AF}} + E_1^{\mathrm{FM}}) = -77.603\ \mathrm{eV} \tag{19}$$

$$E_2^{\mathrm{PM}} = \tfrac{1}{2}(E_2^{\mathrm{AF}} + E_2^{\mathrm{FM}}) = -77.687\ \mathrm{eV} \tag{20}$$

which are the correct values to evaluate the probabilities of the configurations. The probability of occurrence of configuration 1 in the $1 \times 1 \times 2$ supercell then is 18.9%, which is between the values calculated with the FM and the AF energies. We can see in figure 5 that the PM probabilities are closer to the FM and AF values than to the NM results, which suggests that the error introduced by excluding spin polarization is larger than the error contributed by the magnetic ordering when FM or AF energies are used.

3.3. The $2 \times 2 \times 2$ *supercell*

As we also need to study the arrangement of cations in directions perpendicular to the c-axis, we have considered a $2 \times 2 \times 2$ supercell. There are 12 870 cation combinations in this supercell, although we clearly only need to calculate the independent configurations. We have therefore used the SOD program to identify the 180 non-equivalent combinations. The fractional coordinates of the ions were fully relaxed for each configuration, although the cell parameters were kept fixed at the optimized value for configuration 2 in the $1 \times 1 \times 2$ supercell.

Although the evaluation of paramagnetic energies in the $1 \times 1 \times 2$ supercell involved the calculation of both AF and FM energies, we note that for any larger supercell it is now possible to calculate only the FM energies and then use the magnetic coupling constants to evaluate the paramagnetic energies as

$$E^{\mathrm{PM}} = E^{\mathrm{FM}} + 2N_v J_v S^2 + 2N_d J_d S^2 \tag{21}$$

where N_v and N_d are the numbers of vertical and diagonal Fe–Fe pairs, respectively. The resulting energies are shown in figure 6, as a function of, N_v. Out of the 180 different

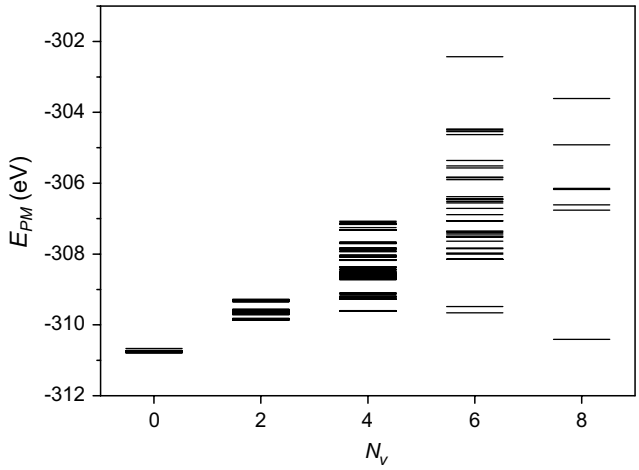

Figure 6. Correlation between the energy E_{PM} and the number N_v of Fe–Fe pairs for the unrelaxed configurations in the $2 \times 2 \times 2$ supercell. The low-energy points at $N_v = 0$ correspond to configurations with total Fe–Sb alternation along the c-direction.

configurations in this supercell, only 11 (those with $N_v = 0$ in) present complete alternation of Fe and Sb along all columns in the c-direction. The results show that, as expected from the $1 \times 1 \times 2$ supercell, these configurations have the lowest energies. Moreover, as a general trend, the smaller the number of vertical Fe–Fe pairs in any given cationic distribution, the more stable the configuration (figure 6). However, there is one configuration with $N_v = 8$, which corresponds to perfect ordering in each unit cell (equivalent to configuration 1 in the supercell $1 \times 1 \times 2$), with an energy comparable to the energy of the configurations with $N_v = 0$. This is a feature that was not found in our previous study of the cation distribution in $FeSbO_4$, but its effect on the cation ordering is negligible, as the degeneracy of this configuration ($\Omega = 2$) is much lower than the accumulated degeneracy of the configurations with $N_v = 0$ ($\sum \Omega = 256$). The accumulated probability of the configurations with $N_v = 0$ calculated at the synthesis temperature is in fact very close to 1, confirming that the alternation of cations along the c-axis is favoured over other cation distributions. The small difference between the 11 configurations with $N_v = 0$ indicates the presence of a large lateral disorder in the distribution. The present results therefore suggest that the cation ordering in $FeSbO_4$ is one-dimensional, in line with our previous results.

3.4. Configurational entropies

Finally, we discuss the behaviour of the configurational entropy, which provides a quantitative measure of the degree of ordering in the system. We used equation (9), and the paramagnetic energies calculated for the $1 \times 1 \times 2$ and $2 \times 2 \times 2$ supercells to obtain the configurational entropies for both supercells, as shown in table 3. At the two temperatures studied, 300 and 1273 K, the entropy of the $1 \times 1 \times 2$ supercell is higher than for $2 \times 2 \times 2$, because the ground state has a degeneracy of four, while the total number of configurations is six. As a result, the system has an entropy close to that of a totally disordered system, in which all the configurations are equally accessible. The table also shows the maximum values of the entropy S_{max} that the supercells would have if it they were completely disordered in that supercell, as calculated from equation (10). Since it has a higher number of possible configurations, S_{max} is

Table 3. Configurational entropies per formula unit (10^{-5} eV K^{-1}) of $FeSbO_4$ at 300 and 1273 K, in comparison with the values expected in a completely disordered system of the same size (S_{max}) and extrapolated to infinite cell size (S_∞).

	S(300 K)	S(1273 K)	S_{max}	S_∞
$1 \times 1 \times 2$	6.30	7.50	7.70	11.95
$2 \times 2 \times 2$	5.68	5.96	10.19	11.95

higher for the $2 \times 2 \times 2$ supercell than for the $1 \times 1 \times 2$ supercell. However, in the larger system there is a small group of configurations, those with $N_v = 0$, which are much more stable than the rest, and therefore the configurational entropy is lower.

The last column in table 3 shows S_∞, which is the maximum value of the entropy (per formula unit) for a given composition. This is the limit of the maximum entropy per formula unit S_{max} when the number of unit cells in the supercell tends to infinity, and it can be obtained from equation (9), where N is the number of configurations of a system with N_s sites, which are occupied by Fe and Sb with equal probability:

$$N = \frac{N!}{(\frac{N_s!}{2})(\frac{N_s!}{2})}. \tag{22}$$

Using Stirling's formula to approximate the logarithms of large numbers, it can be shown that, when the number of sites tends to infinity, the entropy per site is

$$\frac{S_\infty}{N_S} = k_B \ln 2 = 5.975 \times 10^{-5} \text{ eV K}^{-1}. \tag{23}$$

In $FeSbO_4$ there are two sites per formula unit, so the maximum entropy per formula unit that the system can have is 11.95×10^{-5} eV K^{-1}. The configurational entropy that we obtained is considerably lower (5.96×10^{-5} eV K^{-1} in the $2 \times 2 \times 2$ supercell), which is ~50% of S_∞. This entropy reduction indicates the presence of ordering in the system, with two different origins: the size limit of the employed supercell, which imposes a periodic ordering and is responsible for a reduction of 15% of the entropy, and the real effect of cation ordering along the c-axis within the supercell, which is responsible for 35% of the decrease in entropy.

4. Summary

We have presented a methodology for the study of site-occupancy disorder in periodic solids, which makes use of the symmetry information of the system to reduce the size of the configurational space. We have shown that two configurations are equivalent by symmetry if they are related by an isometric operation, and that a trial list of isometric transformations is provided by the group of symmetry operators in the parent structure, that is, the structure from which all configurations are generated via atomic substitutions. We describe how to perform statistics in the reduced space, in order to calculate configurational probabilities and entropies. The equations are basically the same as in the full configurational space, provided that the energy of each configuration is substituted by its reduced energy, which is obtained from the configuration energy by subtracting an entropy-like contribution related to the degeneracy of the independent configuration in the full configurational space.

We present a computer program, SOD (Site-Occupancy Disorder), in which we have implemented an algorithm to obtain the list of non-equivalent configurations from a full list of substitutional combinations. The SOD program can also perform other tasks to assist the multi-configurational modelling, e.g. create input files for simulation programs such as GULP

or VASP, and process the output from these codes to calculate probabilities and thermodynamic variables. The program is available on request from the authors[4].

The present methodology allows an exhaustive investigation of the configurational space in disordered systems even for relatively large supercells, as usually the number of configurations is reduced by some orders of magnitude, depending on the symmetry of the system. In particular, these tools allow the use of *ab initio* techniques to study disorder in systems, which previously were inaccessible to these computationally intensive methods. Moreover, if even larger systems need to be studied, the reduction in the number of configurations achieved by this methodology can also be helpful. For example, it is possible to combine symmetry arguments with Monte Carlo sampling techniques, as it would be even more efficient to sample the reduced configurational space by Monte Carlo techniques; work in this direction is now in progress.

We have illustrated the use of this methodology in the study of the cation distribution in iron antimony oxide $FeSbO_4$, using a more sophisticated level of calculation than in previous studies. We have also described here how to eliminate the contribution of magnetic ordering to the energy differences between configurations, while retaining the spin-polarized nature of the calculations, by using a spin model Hamiltonian to estimate the energies in the paramagnetic phase. The results confirm our previous findings showing that the alternation of Fe and Sb along the *c*-direction of the $FeSbO_4$ crystal is favoured compared to any deviations away from this order. We suggest, therefore, that the crystal structure contains one-dimensional chains of alternating Sb and Fe octahedra which share edges along the *c*-direction, although defective Fe–Fe and Sb–Sb vertical pairs can occur. The lateral connection of these chains seems to be significantly disordered, which could prevent the detection of cation ordering in diffraction studies. As an indication of this partial disorder, the configurational entropy calculated for $FeSbO_4$ is around half the value expected for a completely disordered system with the same composition, although a small fraction of this decrease arises from the finite size of the supercell employed.

Acknowledgments

This work has been supported by the EPSRC under grants GR/S01986/01 and EP/C51744X/01. Computer resources on HPCx were provided via our membership of the Materials Chemistry HPC Consortium and funded by EPSRC (portfolio grant EP/D504872/1). We also thank Dr Jeremy Cockroft for useful discussions.

References

[1] Bosenick A, Dove M T, Heine V and Geiger C A 2001 *Phys. Chem. Minerals* **28** 177
[2] Bosenick A, Dove M T, Myers E R, Palin E J, Sainz-Diaz C I, Guiton B S, Warren M C, Craig M S and Redfern S A T 2001 *Mineral. Magn.* **65** 193
[3] Du Z, De Leeuw N H, Grau-Crespo R, Wilson P B, Brodholt J P, Calleja M and Dove M T 2005 *Mol. Simul.* **31** 339
[4] Grau-Crespo R, Peralta A G, Ruiz-Salvador A R, Gomez A and Lopez-Cordero R 2000 *Phys. Chem. Chem. Phys.* **2** 5716
[5] Islam M S, Driscoll D J, Fisher C A J and Slater P R 2005 *Chem. Mater.* **17** 5085
[6] Khan M S, Islam M S and Bates D R 1998 *J. Mater. Chem.* **8** 2299
[7] Lavrentiev M Y, Allan N L and Purton J A 2003 *Phys. Chem. Chem. Phys.* **5** 2190
[8] Lavrentiev M Y, Purton J A and Allan N L 2003 *Am. Mineral.* **88** 1522
[9] Purton J A, Lavrentiev M Y and Allan N L 2005 *J. Mater. Chem.* **15** 785

[4] Please E-mail Dr Ricardo Grau-Crespo <r.grau-crespo@ucl.ac.uk>

[10] Todorov I T, Allan N L, Lavrentiev M Y, Freeman C L, Mohn C E and Purton J A 2004 *J. Phys.: Condens. Matter* **16** S2751
[11] Metropolis N, Rosenbluth A W, Rosenbluth M N, Teller A H and Teller E 1953 *J. Chem. Phys.* **21** 1087
[12] Grau-Crespo R, de Leeuw N H and Catlow C R A 2003 *J. Mater. Chem.* **13** 2848
[13] Grau-Crespo R, de Leeuw N H and Catlow C R A 2004 *Chem. Mater.* **16** 1954
[14] Giacovazzo C 2002 *Fundamentals of Crystallography* 2nd edn (Oxford: Oxford University Press)
[15] Berlepsch P, Armbruster T, Brugger J, Criddle A J and Graeser S 2003 *Mineral. Magn.* **67** 31
[16] Dove M T 1993 *Introduction to Lattice Dynamics* (Cambridge: Cambridge University Press)
[17] Farber L, Matjaz Valant M, Akbas M A and Davies P K 2002 *J. Am. Ceram. Soc.* **85** 2319
[18] Berry F J, Holden J G and Loretto M H 1986 *Solid State Commun.* **59** 397
[19] Berry F J, Holden J G and Loretto M H 1987 *J. Chem. Soc. Faraday Trans.* **83** 615
[20] Kresse G and Furthmuller J 1996 *Comput. Mater. Sci.* **6** 15
[21] Kresse G and Furthmuller J 1996 *Phys. Rev.* B **54** 11169
[22] Kresse G and Hafner J 1993 *Phys. Rev.* B **48** 13115
[23] Kresse G and Hafner J 1994 *J. Phys.: Condens. Matter* **6** 8245
[24] Perdew J P and Zunger A 1981 *Phys. Rev.* B **23** 5048
[25] Vosko S H, Wilk L and Nusair M 1980 *Can. J. Phys.* **58** 1200
[26] Perdew J P 1992 *Phys. Lett.* A **165** 79
[27] Blochl P E 1994 *Phys. Rev.* B **50** 17953
[28] Kresse G and Joubert D 1999 *Phys. Rev.* B **59** 1758
[29] Anisimov V I, Zaanen J and Andersen O K 1991 *Phys. Rev.* B **44** 943
[30] Rohrbach A, Hafner J and Kresse G 2003 *J. Phys.: Condens. Matter* **15** 979
[31] Liechtenstein A I 1995 *Phys. Rev.* B **52** R5467
[32] Dudarev S L, Botton G A, Savrasov S Y, Humphreys C J and Sutton A P 1998 *Phys. Rev.* B **57** 1505
[33] Solovyev I V, Dederichs P H and Anisimov V I 1994 *Phys. Rev.* B **50** 16861
[34] Grau-Crespo R, Cora F, Sokol A A, de Leeuw N H and Catlow C R A 2006 *Phys. Rev.* B **73** 035116
[35] Grau-Crespo R, Catlow C R A and De Leeuw N H 2007 *J. Catal.* **248** 77
[36] Grau-Crespo R, Moreira I D R, Illas F, de Leeuw N H and Catlow C R A 2006 *J. Mater. Chem.* **16** 1943